Journal of Manufacturing Processes 68 (2021) 1147–1157

Contents lists available at ScienceDirect

Journal of Manufacturing Processes

journal homepage: www.elsevier.com/locate/manpro

The tribology between monocrystalline diamond and polycrystalline cubic boron nitride during frictional contact

Ulrich Müller [a,*], Josef Kaiser [a], Sebastian Barth [a], Thomas Bergs [a,b]

[a] Laboratory for Machine Tools and Production Engineering (WZL), RWTH Aachen University, Campus-Boulevard 30, 52074 Aachen, Germany
[b] Fraunhofer Institute for Production Technology IPT, Steinbachstraße 17, 52074 Aachen, Germany

ARTICLE INFO

Keywords:
Tribology
Grinding
Polycrystalline cubic boron nitride
Diamond
Friction

ABSTRACT

The abrasive machining of superhard cutting tool materials such as polycrystalline cubic boron nitride is often conducted by grinding using diamond grinding wheels. Due to the high grinding wheel wear and the low material removal rates during grinding of polycrystalline cubic boron nitride, the manufacturing of this superhard material causes high production costs. The investigation of the tribology between diamond and polycrystalline cubic boron nitride enables to identify the cause-effect-relationships in the contact zone of the grinding wheel and the workpiece and thus to increase the process efficiency due to a knowledge-based process design. Hence, this paper presents an approach for the measurement of tribological process state variables and an empirical-analytical model to describe the tribological behavior during frictional contact of polycrystalline cubic boron nitride and diamond in cutting processes. The empirical-analytical model enables to calculate tribological process state variables such as the temperature of contact depending on the process input variables and the material properties of polycrystalline cubic boron nitride.

1. Introduction

1.1. Background

In the automotive and aerospace industries, machining processes are constantly optimized to increase efficiency. Hence, a trend towards the use of superhard cutting materials such as polycrystalline cubic boron nitride (pcBN) and polycrystalline diamond (PCD) is observed [1]. Cutting materials are often classified according to toughness and strength. Superhard cutting materials have the highest strength but low toughness compared to conventional cutting materials such as cemented carbides and high speed steel [2]. The properties of superhard cutting materials enable high cutting rates and increased tool life, which offer potential for increasing process efficiency [3]. Diamond and cBN single crystals are therefore often used as superabrasives for grinding of hard-to-machine materials such as gamma titanium [4] and nickel based alloys [5]. Furthermore, the automotive and aerospace industries are pushing the research and application of new and advanced materials, which are often hard-to-machine with conventional cutting materials due to the high hardness and strength [30]. Therefore, PCD and pcBN are increasingly used for machining with geometrically defined cutting edge of new materials such as metal matrix [6], fiber reinforced composites [7], nickel based alloys [8] and titanium alloys [9]. In addition, pcBN is applicable for the machining of ferrous alloys due to the high chemical and thermal stability of pcBN, whereas PCD is not due to its chemical affinity to ferrous [10]. A disadvantage of using pcBN as a cutting material are the higher costs compared to conventional cutting materials. Therefore, different approaches to reduce the costs of pcBN have been researched. Manufacturers are constantly improving the physical properties of the cBN grains and the binder respectively matrix composition. This allows the pcBN to be selected according to the machining task and thus offers the potential to increase the productivity of the machining process when using pcBN as cutting tool material [11]. In addition, a process-specific cutting edge geometry was found to increase the productivity of machining with pcBN cutting tools [12]. Furthermore, research is carried out to reduce manufacturing costs of pcBN cutting tools. This was achieved by integrating cutting edge preparation into the grinding process [13] and by combining grinding and laser beam processes [14]. The grinding process accounts for 45 to 60% of the finishing costs of pcBN cutting tools [15]. Grinding therefore still offers great potential for reducing manufacturing costs through knowledge-based grinding process design.

* Corresponding author.
E-mail address: u.mueller@wzl.rwth-aachen.de (U. Müller).

https://doi.org/10.1016/j.jmapro.2021.06.026
Received 18 March 2021; Received in revised form 10 June 2021; Accepted 11 June 2021
Available online 29 June 2021

Nomenclature

A_{MCD}	Cross-sectional area of MCD, [mm^2]	K_{Ic}	Fracture toughness, [MPa·m$^{1/2}$]
c_s	Spring rate, [N/mm]	n_s	Rotational speed, [1/min]
d_{cBN}	cBN grain size, [µm]	P_c	Grinding power, [W]
d_{blank}	Diameter of blank holder, [mm]	P_f	Friction power, [W]
d_{pyro}	Diameter of erosion bore, [µm]	Ra	Arithmetic mean roughness, [µm]
E	Modulus of elasticity, [GPa]	R_{ch}	Edge chipping roughness, [µm]
F_f	Friction force, [N]	T	Contact temperature, [°C]
F_n	Normal force, [N]	T_p	Process temperature, [°C]
$F_{n,stat}$	Static normal force, [N]	v_c	Cutting speed, [m/s]
F_{pre}	Preload force, [N]	v_f	Feed rate, [mm/min]
F_t	Tangential force, [N]	v_{rel}	Relative velocity, [m/s]
H_K	Knoop hardness, [GPa]	v_w	Workpiece velocity, [mm/min]
H_{pcBN}	pcBN hardness, [GPa]	w_{cBN}	cBN content, [%]
		λ	Thermal conductivity, [W/m·K]
		μ	Coefficient of friction

1.2. Grinding of superhard materials

Mamalis investigated the grinding wheel wear during grinding of superhard and polycrystalline materials such as PCD and pcBN [16]. He found that depending on the height of grains over bond grain break out and grain flattening were dominant mechanisms of the grinding wheel wear. Further investigations on grinding wheel wear during grinding of pcBN were conducted by Behrens [17]. According to Behrens, the major wear mechanism in productive grinding of pcBN was grain splintering but also grain break out and friction due to grain flattening were found as wear mechanisms. Behrens also investigated the material removal mechanisms during grinding of pcBN and observed that mainly brittle material removal mechanisms occurred. Furthermore, Ventura investigated different grinding strategies in order to optimize the cutting edge preparation of pcBN inserts [13]. He observed that edge chipping and surface roughness of the ground pcBN inserts were related to the diamond abrasive grain size. In addition, Ventura found that the grinding wheel wear and the material removal mechanisms depended on the pcBN specification and thus on the grain size and amount of cBN. Smaller cBN grains and lower cBN amount caused an increased edge chipping on the ground inserts at constant grinding parameters. Mao et al. investigated material removal mechanisms during grinding of composite materials made of cBN and WC-Co cemented carbides [18]. Mao et al. observed a transition from ductile to brittle material removal of the WC-Co matrix when the chip thickness increased due to a higher feed rate of the grinding wheel. According to Mao et al., the cBN grains were always machined brittle. Haenel et al. investigated the grinding of binderless nanocrystalline cubic boron nitride BNNC [19]. According to Haenel et al., the BNNC consisted of cBN without any matrix but with small amount of hexagonal boron nitride remained from the phase transition during manufacturing of the BNNC blank. Due to the higher hardness of the BNNC, 400% higher forces resulted when grinding with diamond grinding wheels compared to a conventional pcBN. Brittle machining of the BNNC workpieces was found to be the major material removal mechanism. Denkena et al. investigated the influence of the cutting direction angle during grinding of pcBN [20]. According to Denkena et al., an increased cutting direction angle of the grinding wheel resulted in a decreased profile wear of the grinding wheel.

1.3. Tribological conditions during grinding of superhard materials

Since friction in the contact zone between the abrasive grains and the workpiece is an essential driver of the grinding wheel wear [17], researchers have been focusing on the tribological conditions between the abrasive grains of a grinding wheel and superhard materials. In order to investigate the tribological conditions during grinding of PCD, Vits et al. developed a single grain friction test rig [21]. According to Vits et al., an increased contact force F_n resulted in an increased friction coefficient μ (Eq. (1)).

$$\mu(F_n) = 3 \times 10^{-6} F_n^2 - 3.1 \times 10^{-4} F_n + 0.1053 \quad (1)$$

Bergs et al. transferred the findings of Vits et al. to a multigrain contact in additional investigations [22]. This was achieved by conducting grinding tests with ceramic-bonded diamond grinding wheels considering the same PCD specifications. According to Bergs et al., the grinding power P_c can be calculated by the fracture toughness K_{Ic} of the PCD, the relative velocity v_{rel} between the abrasive grain and the PCD workpiece, the friction law $\mu(F_n)$ developed by Vits et al. (Eq. (1)) and the contact force F_n. Subsequently, the grinding power P_c (Eq. (2)) was used to calculate the process temperature T_p (Eq. (3)).

$$P_c = (-0.0147 K_{Ic} + 1.3481) \times \mu(F_n) \times v_{rel} \times F_n \quad (2)$$

$$T_p(P_c) = 0.2633 \times P_c + 47.443 \quad (3)$$

1.4. Scientific problem statement

The previously discussed references have in common that no quantitative models were developed in order to describe the thermal load during grinding of pcBN [13,16–20]. Furthermore, the existing investigations on tribological conditions during grinding of superhard materials only considered the contact between an abrasive grain and PCD but not between an abrasive grain and pcBN [21,22]. Therefore, the tribological conditions and thus the thermal load in the contact zone during grinding of pcBN are currently unknown. However, knowledge of the tribological conditions offers the potential to reduce grinding wheel wear and to prevent damage to the workpiece material subsurface due to excessive thermal load. Since measurement of tribological conditions between single abrasive grains in the contact zone during grinding is prone to errors and virtually impossible, tribological investigations need to be conducted separately. Therefore, the investigation of the tribological conditions during frictional contact of monocrystalline diamond (MCD) and pcBN offers the potential to identify cause-effect-relationships, which are relevant to the grinding wheel wear.

The presented work contributes to close this knowledge gap by analyzing the tribological conditions during grinding of pcBN. Therefore, the single grain contact between pcBN and MCD was investigated. The influence of the contact force F_n and the relative velocity v_{rel} on the friction coefficient μ and the contact temperature T during sliding contact between MCD and pcBN was investigated and quantitatively described.

2. Materials and methods

The methodology of the present research approach is shown in Fig. 1. First, a control unit based on a Spring-Damper-Unit was configured to enable the systematic variation of the normal force F_n on a 5-axis grinding machine tool. Subsequently, experimental tests were conducted by using a pin-on-disc setup where MCD served as a pin and pcBN as a disc. During the tests, two types of sensors, a dynamometer and a pyrometer, measured the influence of the input variables relative velocity v_{rel}, normal force F_n and pcBN specification on the output variables friction force F_f and contact temperature T. These output variables were used to model the tribological conditions in the contact zone between MCD and pcBN.

2.1. Configuration of the test rig

Fig. 2 shows the configuration of the friction test rig. The friction test rig was designed as a pin-on-disk method according to Vits et al., in which a stationary load can be applied to a rotating disk [21]. The friction samples (Fig. 2, label 3) were modified single grain MCD dressers with a cross-section area of $A_{MCD} = 1.21\ mm^2$ (Fig. 2, label 2), which were clamped in a cylindrical holder (Fig. 2, label 4). The glass fiber of the single-color pyrometer (Fig. 2, label 6) was also clamped in the cylindrical holder. The single grain dresser had an erosion bore with a diameter of $d_{pyro} = 800$ µm, into which the glass fiber of the single-color pyrometer of the type 3ML made by Optris GmbH was inserted. The front surface of the glass fiber was aligned to the bottom of the MCD aiming towards the contact zone. Since MCD is ideally transparent for most of the electromagnetic wavelength spectrum [10], it can be assumed that the measured temperature corresponded very closely to the temperature in the contact zone between the friction sample and the pcBN-blank. The pyrometer was calibrated by the emission coefficient of the pcBN-blanks and validated by reference measurements using a thermocouple type K. The measuring range of the pyrometer was $50\ °C \leq T \leq 400\ °C$.

The base plate for fixing the diamond sample holder and the pyrometer fiber holder was connected via a linear guide (Fig. 2, label 5) to a multi-component force dynamometer of type 9119AA2 made by Kistler Instrumente AG (Fig. 2, label 9). The force dynamometer measured the force components in the three spatial directions. The calibration of each force component of the force dynamometer was conducted according to the manufacturer's calibration certificate and the forces were validated by application and evaluation of reference load. The entire assembly was integrated into a 5-axis tool grinding machine of type S22P turbo from ISOG Technology GmbH. Due to the linear guidance, a freedom of movement of the base plate with the diamond friction sample holder in vertical direction was realized. Below the linear guidance, a Spring-Damper-Unit was mounted. An elastomer damper (Fig. 2, label 7) reduced the process vibrations. With the aid of a helical compression spring (Fig. 2, label 8), specific contact forces were set on the diamond friction sample depending on the linear deflection of the base plate. The stiffness of the Spring-Damper-Unit was $c_s = 46.2$ N/mm and was preloaded with a preload force $F_{pre} = 20$ N. The machine spindle was equipped with a sample holder for the pcBN-blanks (Fig. 2, label 1) with a diameter $d_{blank} = 70$ mm.

2.2. Design of experiments

The experimental design of the single grain friction tests is shown in Fig. 3. The single grain friction tests were carried out without lubricant and along the grinding direction of the MCD. According to the 3^3 Factorial Design shown in Fig. 3, the normal force F_n, the relative velocity v_{rel} and the pcBN specification were varied. The properties of the three considered pcBN specifications are shown in Table 1. The factor stages of the relative velocity were $v_{rel} = 5$; 10; 15 m/s by varying the revolutions per minute n_s of the grinding spindle. The variation of the normal force F_n was achieved by a vertical infeed of the pcBN-blank via the machine spindle at a constant feed rate of $v_f = 1$ mm/min (Control unit, Fig. 1). The vertical spindle feed caused the diamond sample holder to deflect along the linear guidance and the helical compression spring attached underneath it to compress. This enabled a linear temporal increase of the normal force F_n from the preload force F_{pre} to a specific holding force $F_{n,stat}$. The holding force was increased in three steps starting from $F_{n,stat} = 30$ N. At each repetition of a test point, the holding force was increased by $\Delta F_{n,stat} = 20$ N to $F_{n,stat} = 50$ N, and to $F_{n,stat} = 70$ N (Appendix A). The maximum normal force during the friction test of DBW85 was limited to $F_n = 65$ N due to machine overload and MCD damage.

The pcBN-blanks made by Element Six UK Ltd. were semi-finished products for the production of cutting tool inserts. The pcBN specifications DCN450, DCX650 and DBW85 differed in average cBN grain size $d_{g,cBN}$, cBN fraction w_{cBN} and binder phase respectively matrix composition according to Table 1 [24]. Due to the fact, that characterization of superhard materials is challenging, the material properties provided by the manufacturer may vary in a small range but the trends between the considered pcBN specifications were assumed to be realistic. The microstructure of the pcBN specifications is shown in Appendix B. The binder phase of both DCN450 and DCX650 is of ceramic nature whereas the binder phase of DBW85 is rather of metallic nature. Due to the considerably smaller thermal conductivity of titanium carbonitride (TiCN) and titanium nitride (TiN) in the range of $\lambda < 30$ W/m·K compared to pure cBN with $\lambda > 600$ W/m·K [25], the average thermal conductivity λ of pcBN decreases with decreasing fraction of cBN w_{cBN} (Table 1). Furthermore, the hardness H_K of pcBN increases with increasing cBN fraction w_{cBN} but also the binder phase composition as well as the cBN grain size influence the mechanical properties such as the fracture toughness K_{Ic} and the Young's modulus E.

3. Results

3.1. Frictional contact of MCD and pcBN

Fig. 4 shows the influence of the pcBN specification, the normal force F_n and the relative velocity v_{rel} on the friction coefficient μ and the friction force F_f. According to Fig. 4, an increased normal force F_n leads to an increased friction force F_f and thus to a decreased friction coefficient μ. Furthermore, an increased relative velocity v_{rel} caused a decreased friction coefficient μ. During the friction tests with DCX650,

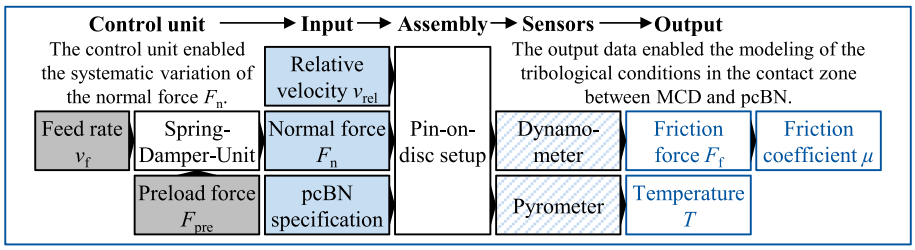

Fig. 1. Methodology.

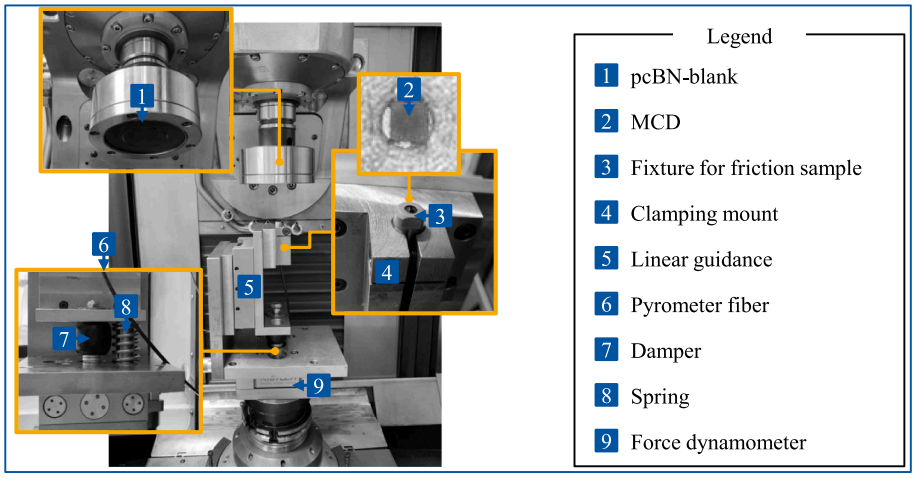

Fig. 2. Configuration of the friction test rig.

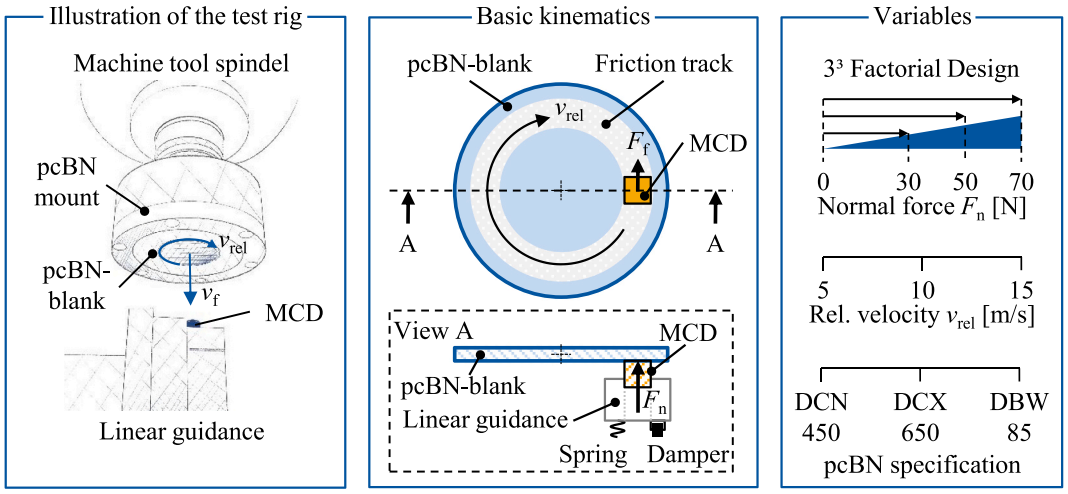

Fig. 3. Design of experiments.

Table 1
Material properties of polycrystalline cubic boron nitride and monocrystalline diamond [24].

Property	Formula symbol	Unit	DCN450	DCX650	DBW85	MCD
cBN grain size	$d_{g,cBN}$	[µm]	< 1	3[a]	2	–
cBN content	w_{cBN}	[%]	45	65	85	–
Binder/Matrix	–	[–]	TiCN	TiN	AlWCoB	–
Knoop hardness	H_K	[GPa]	24.5	24.9	27.5	80–120
Young's modulus	E	[GPa]	646	620	574	1141
Fracture toughness	K_{Ic}	[MPa·m$^{1/2}$]	2.9	5.5	4.9	3.4
Thermal conductivity	λ	[W/m·K]	32.8	52.6	87.5	2000
ISO 513 group			BL	BL	BH	

[a] Multi-modal grain size.

the MCD pin cracked and was replaced by an equal one (Appendix E). The friction tests with the cracked MCD resulted in a spontaneous increase of the friction force F_f and thus the friction coefficient μ. Since the data points related to the cracked MCD were only shifted to a higher level but followed a similar trend as before cracking, these data points were interpreted as an ongoing trend. The influence of the pcBN specification on the friction coefficient μ and on the friction force F_f did not follow a specific trend. This was most likely due to the different binder phase compositions, cBN grain sizes $d_{g,cBN}$ and cBN fractions w_{CBN} (Table 1, Appendix B). Since the friction coefficient μ of DCN450 was considerably less than that of DCX650 and DBW85, the surfaces of the frictions tracks were further investigated. The influence of chemical reactions on the friction coefficient is unlikely due to the thermal and chemical stability of both friction partners under the given temperature conditions.

In order to explain the characteristics of the friction coefficient μ, the surface texture of the friction track on the pcBN-blanks was analyzed by digital microscope images (Appendix F) and the profile method for surface textures according to the international standard ISO 13565-2 [26]. Surface imperfections and characteristics on the friction track were subsequently identified with respect to the international standard ISO 8785 [27]. However, two major differences were observed on the

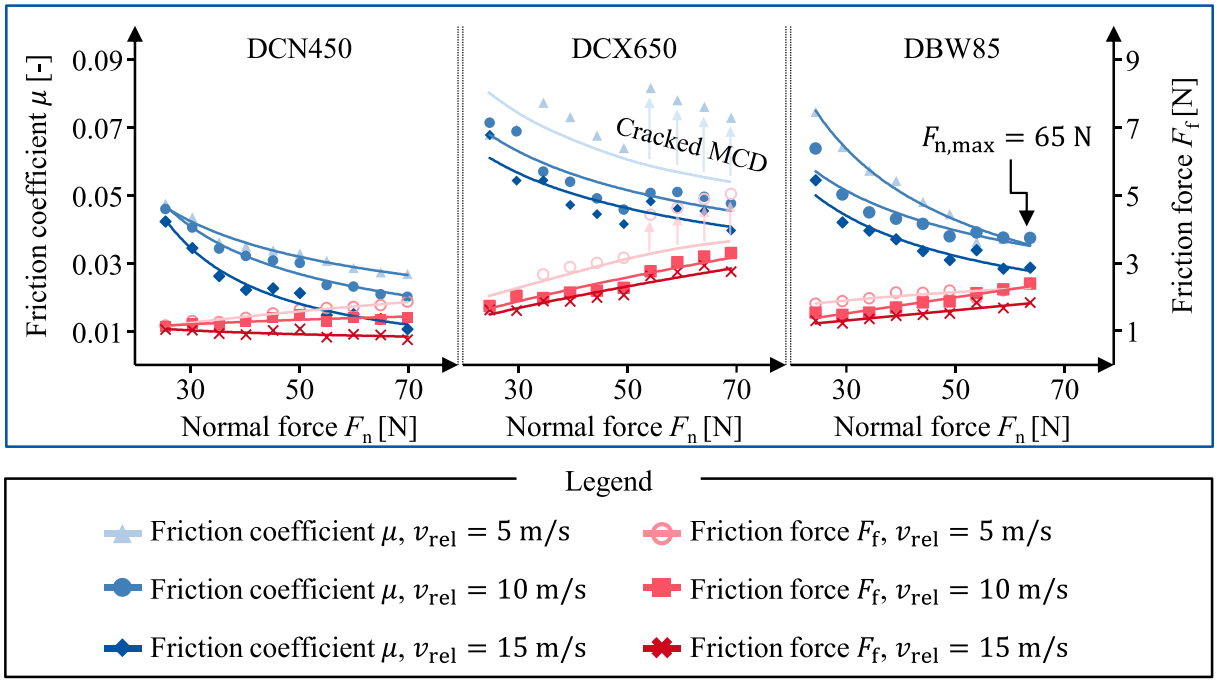

Fig. 4. Influence of the normal force F_n on the friction coefficient μ and friction force F_f depending on the pcBN specification.

pcBN surfaces after the friction tests were conducted. First, the surface texture of DCN450 showed several mechanical stress related imperfections. Second, the surface texture of both DCX650 and DBW85 was found to be minor influenced by the mechanical and thermal load during the friction tests. Fig. 5, label a, shows the roughness profile of the pcBN-blanks evolved during the frictional contact with MCD. The core roughness depth *Rk* and the reduced peak height *Rpk* of the pcBN-blanks were considerably decreased during frictional contact with MCD, which can be attributed to mechanical flattening of roughness peaks (Fig. 5, label a). The evolving surface profiles of the pcBN-blanks were qualitatively illustrated and are shown in Fig. 5, label b. The friction tracks of DCX650 and DBW85 showed no conspicuous changes except the

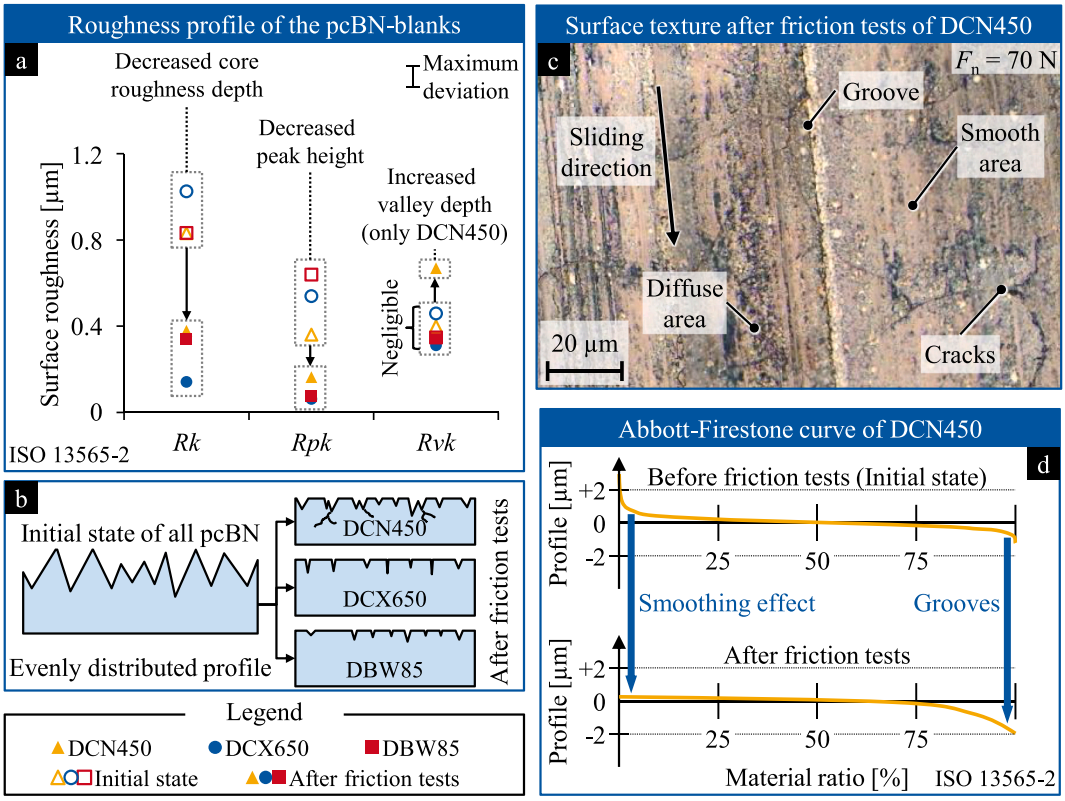

Fig. 5. Roughness profile of the pcBN-blanks before and after the friction tests (a), illustration of the surface texture of the friction track on the pcBN-blanks (b), surface texture of DCN450 after friction tests (c), Abbott-Firestone curve of DCN450 (d).

flattening of the roughness peaks. The reduced valley depth *Rvk* only considerably increased on the surface of DCN450, whereas both DCX650 and DBW85 showed negligible increased reduced valley depths *Rvk*. This can be explained by the surface texture of the friction track of DCN450 after the friction tests (Fig. 5, label c) and the related Abbott-Firestone curve (Fig. 5, label d). Surface imperfections such as grooves and cracks were found on the friction track of DCN450, which most likely are related to the lower hardness H_K and fracture toughness K_{Ic} compared to DCX650 and DBW85. Furthermore, smooth areas were found on the friction track of DCN450 indicating "plastic flow". Both the grooves and the smooth areas were clearly indicated by the characteristics of the Abbott-Firestone curve of the friction track of DCN450 (Fig. 5, label d).

However, the quasi-plastic deformation of brittle materials was previously reported by Lawn et al. [28] and Bifano et al. [29]. According to Lawn et al., the nature of the irreversible deformation in otherwise brittle materials originates from shear faults in the grain microstructure when large compressive stress is applied [28]. Bifano et al. stated that "*all brittle materials will undergo plastic flow rather than fracture if the depth of machining is small enough*" [29]. Therefore, the mechanical load applied to DCN450 during the friction tests apparently represented the transition from brittle to ductile material behavior. The occurrence of "plastic flow" may explains the lower friction force F_f during frictional contact of DCN450 and MCD compared to DCN650 and DBW85. This phenome also effected the temperature *T* in the contact zone during the friction tests. Hence, the energy dissipation and the temperature of contact was analyzed in Section 3.2.

3.2. Energy dissipation and temperature of contact

The influence of the pcBN specification, the normal force F_n and the relative velocity v_{rel} on the friction power P_f and the contact temperature *T* is shown in Fig. 6. The friction power P_f was calculated by the friction force F_f and the relative velocity v_{rel} according to Formula (4).

$$P_f(F_n v_{rel}) = F_f(F_n v_{rel}) \times v_{rel} \quad (4)$$

No obvious dependency of the pcBN specification on the friction power P_f and the contact temperature *T* was found but the contact temperature *T* of the ceramic bonded DCN450 and DCX650 was higher at similar friction power P_f compared to DBW85. The highest friction power P_f and the highest contact temperatures *T* were measured with the pcBN specification DCX650. The friction power P_f was 82% higher on average and the contact temperature *T* was 20% higher on average than for the pcBN specifications DCN450 and DBW85.

The results of the friction power P_f can be explained by the relationship shown in Formula (4) and the explanatory approaches from Fig. 5 considering the surface characteristics of the friction track as follows. In order to explain the results of the contact temperature *T*, Fig. 7 shows two linear relationships between the friction power P_f and the contact temperature *T*. With increasing friction power P_f, the contact temperature *T* increased, since a large part of the friction power P_f dissipates into heat. On the friction track of DCN450 (a), the contact temperature *T* most likely increased faster than on DCX650 and DBW85 due to the lower thermal conductivity λ (Table 1) and the previously discussed quasi-plastic deformation (Section 3.1). While the lower thermal conductivity λ results in accumulation of heat in the contact zone and thus leads to higher contact temperatures *T*, the quasi-plastic deformation goes along with temperature increasing inner friction. Hence, the contact temperature *T* of DCN450 increases faster compared to DCX650 and DBW85 due to the different material behavior occurring during frictional contact with MCD.

3.3. Synthesis of findings

For the synthesis of the findings, a qualitative overview of the results is shown in Fig. 8. Hence, qualitative trends were derived from the previously described diagrams in the Sections 3.1 and 3.2. In addition, for each target parameter a mathematical approach was developed. The friction coefficient μ can be described as a function *f* of the process input

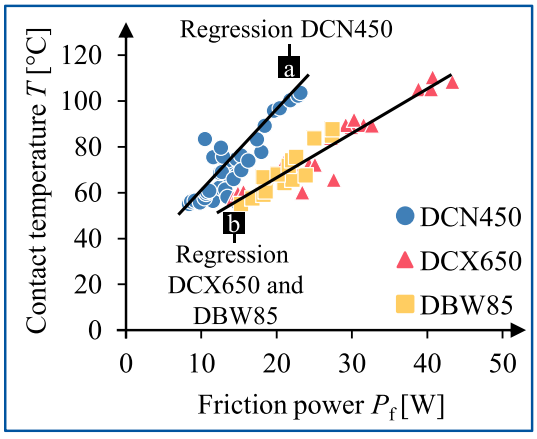

Fig. 7. Calculation of the contact temperature T by the friction power P_f.

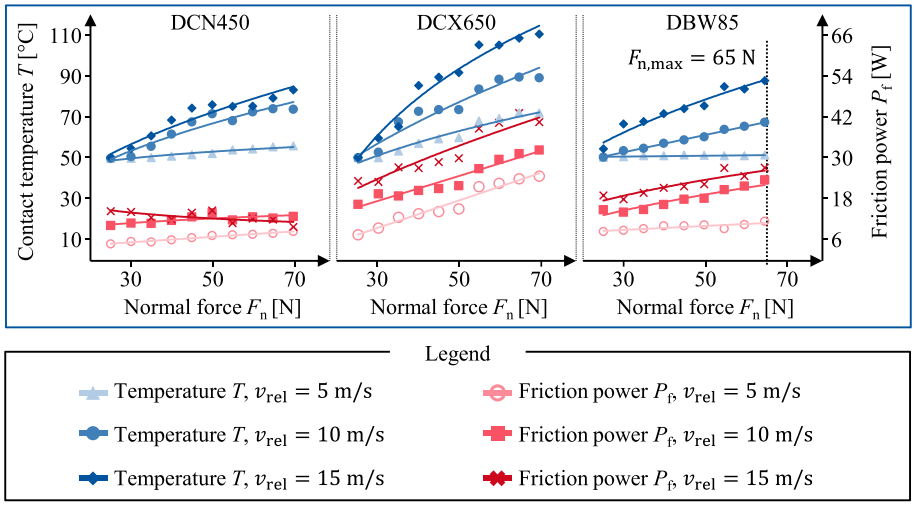

Fig. 6. Influence of the normal force F_n on the contact temperature T and the friction power P_f depending on the pcBN specification.

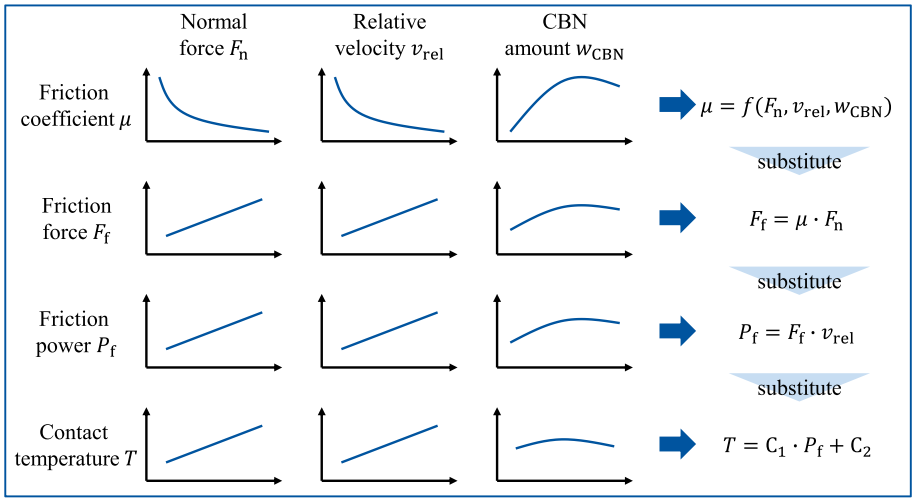

Fig. 8. Qualitative overview of the results and mathematical modeling approach.

variables normal force F_n and relative velocity v_{rel} as well as material related parameters such as the cBN amount w_{cBN}. Furthermore, Coulomb's law of friction was chosen to consider the friction force F_f. The friction power P_f can be expressed by the product of friction force F_f and relative velocity v_{rel} [21]. According to Fig. 7, the contact temperature T can be calculated by the friction power P_f using a linear function.

Fig. 9 shows four different mathematical models of the friction coefficient μ of the pcBN specification DCN450. First, a linear function was chosen to fit the measured values (Fig. 9, label a). Due to relatively large deviations between the experimental data and the calculated values of the linear model (up to 20.3%), two modified exponential functions were subsequently used whereas the first model considered both the cBN amount w_{cBN} and the fracture toughness K_{Ic} as material properties (Fig. 9, labels b and c). The second exponential model only considered the fracture toughness K_{Ic} and less complex coefficients (Fig. 9, label c). In addition, a modified power function was adopted as a fourth model (Fig. 9, label d). The lowest average deviation (<10%) between the calculated and the measured values was generated from the complex exponential function, which considered two pcBN material properties (Fig. 9, label b). Hence, this model was chosen for further development. Furthermore, polynomial approaches for modeling the friction coefficient μ, which were used in previous studies [23], can only be extrapolated to a limited extent due to the unlimited nature of these functions, taking into account a reasonable range of validity.

Formula (5) shows the aforementioned exponential model for the friction coefficient μ. The range of validity of the developed model is limited by the coefficient functions $K(K_{Ic})$, $A(K_{Ic})$ and $B(w_{cBN})$, since these functions include natural boundaries. According to Formula (6) and (7), the fracture toughness K_{Ic} was considered by the arctangent functions $K(K_{Ic})$ and $A(K_{Ic})$. Formula (8) shows the function which considered the cBN amount $B(w_{cBN})$. The optimized values for $K(K_{Ic})$, $A(K_{Ic})$ and $B(w_{cBN})$ were given by Appendix C. The fracture toughness K_{Ic} was chosen as a variable for the friction model in order to represent the differences of the binder phase composition (ceramic/metallic) and cBN grains in a single variable. In addition, the fraction of cBN w_{cBN} was considered due to its correlation to the hardness H and to the thermal conductivity λ of pcBN. Therefore, the friction models takes physical relationships between the tribological behavior and material properties into account.

$$\mu = f(F_n, v_{rel}, w_{cBN}, K_{Ic}) = K(K_{Ic}) \times \left(1 + A(K_{Ic}) \times exp\left(-\left(B(w_{cBN}) \times F_n^2 \times v_{rel}\right)\right)\right) \quad (5)$$

$$K(K_{Ic}) = a_1 \times arctan((b_1 \times K_{Ic} - c_1) + \pi/2)) \quad (6)$$

$$A(K_{Ic}) = a_2 \times arctan((b_2 \times K_{Ic} - c_2) - \pi/2)) \quad (7)$$

$$B(w_{cBN}) = a_3 \times w_{cBN}^{b_3} \quad (8)$$

The output of the empirical-analytical friction model (5) is shown in Fig. 10 for all three considered pcBN specifications. In addition, the set of curves for the friction force F_f, the friction power P_f and the contact temperature T based on the equations shown in Fig. 8 are given by Fig. 10. The set of curves was calculated for the relative velocity $v_{rel} = 5$; 10; 15 m/s. As shown before, the experimental tests with the pcBN specification DCX650 were partially conducted using a cracked MCD (Fig. 4). This resulted in a higher deviation of the friction model

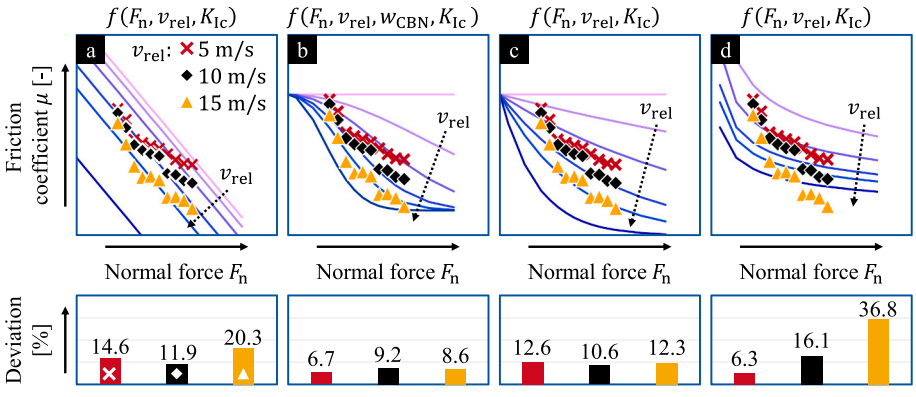

Fig. 9. Comparison of different mathematical models for the friction coefficient μ of DCN450.

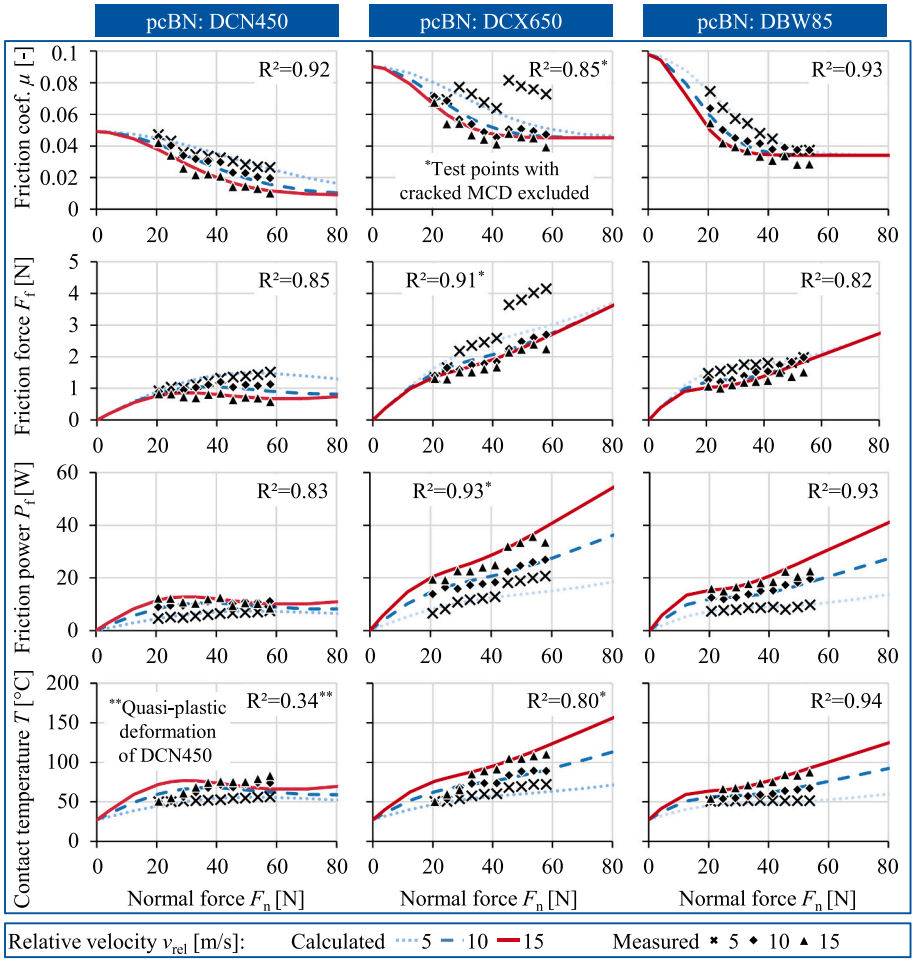

Fig. 10. Results of the empirical-analytical friction model.

compared to the other two pcBN specifications. However, the overall deviation between the measured values and the values calculated by the friction model was 8.3% on average. In comparison, the deviation of the calculation of the friction coefficient μ, the friction force F_f, the friction power P_f and the contact temperature T was in the range of 2.9–17% for DCN450, 5.9–16.6% for DCX650 and 3.2–8.7% for DBW85 (Appendix D). For better comparison, the determination coefficients R^2 were calculated for each model, whereas the test points conducted with a cracked MCD were excluded. All models showed a determination coefficient of $R^2 \geq 0.8$, except the strongly on the quasi-plastic deformation dependent contact temperature T of DCN450. The poor quality of the model for the contact temperature T of DCN450 is most likely due to the different characteristics of heat transfer on the friction track compared to the harder pcBN specifications, which can be derived from Fig. 7. Therefore, ongoing research will be conducted in this area in order to improve the quality of the model and thus enable a valid prediction of the contact temperature T.

4. Conclusion

The work presented in this paper showed a successful application of a test rig for tribological investigations using a 5-axis tool grinding machine tool. Furthermore, it can be stated, that different characteristics of tribology occur during the frictional contact of MCD and pcBN. The friction coefficient was less than $\mu = 0.1$ for all test points, indicating that the contact between MCD and pcBN is characterized by very low friction. It was found, that an increased normal force F_n and an increased relative velocity v_{rel} lead to a decreased friction coefficient μ. In addition, the pcBN specification showed a significant influence on the friction between MCD and pcBN, whereas an increased fracture toughness K_{Ic} of pcBN resulted in an increased friction coefficient μ. The tribological behavior of the frictional contact of MCD and pcBN can be expressed by an empirical-analytical model, which is based on an exponential function describing the friction coefficient μ in dependence of the normal force F_n, the relative velocity v_{rel} as well as the material properties fracture toughness K_{Ic} and cBN amount w_{cBN}. Hence, the findings presented in this paper allow a dedicated view on the contact zone between MCD and pcBN in grinding processes. Since the measurement of temperatures and friction in the contact zone between the abrasive grains and the workpiece during grinding is yet impossible, the dedicated view contributes to the optimization of grinding of superhard materials due to the knowledge of the cause-effect-relationships in the contact zone.

Declaration of competing interest

The authors declare that they have no known competing financial interests or personal relationships that could have appeared to influence the work reported in this paper.

Acknowledgements

The authors thank the German Research Foundation (DFG) for funding the present research in the project “Analysis of material removal mechanisms in grinding of super hard cutting materials regarding polycrystalline cubic boron nitride (pcBN)” (BE2542/19-2).

Appendix A. Method for the evaluation of the results

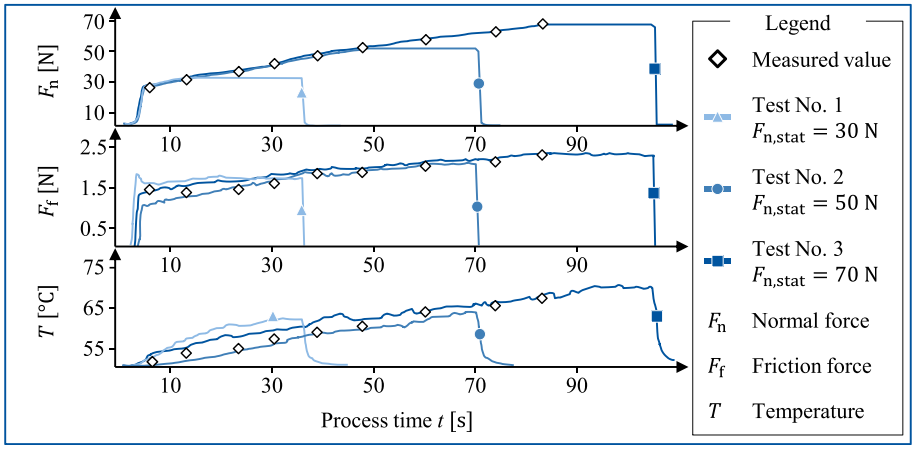

Appendix B. SEM images of the pcBN specifications DCN450, DCX650 and DBW85

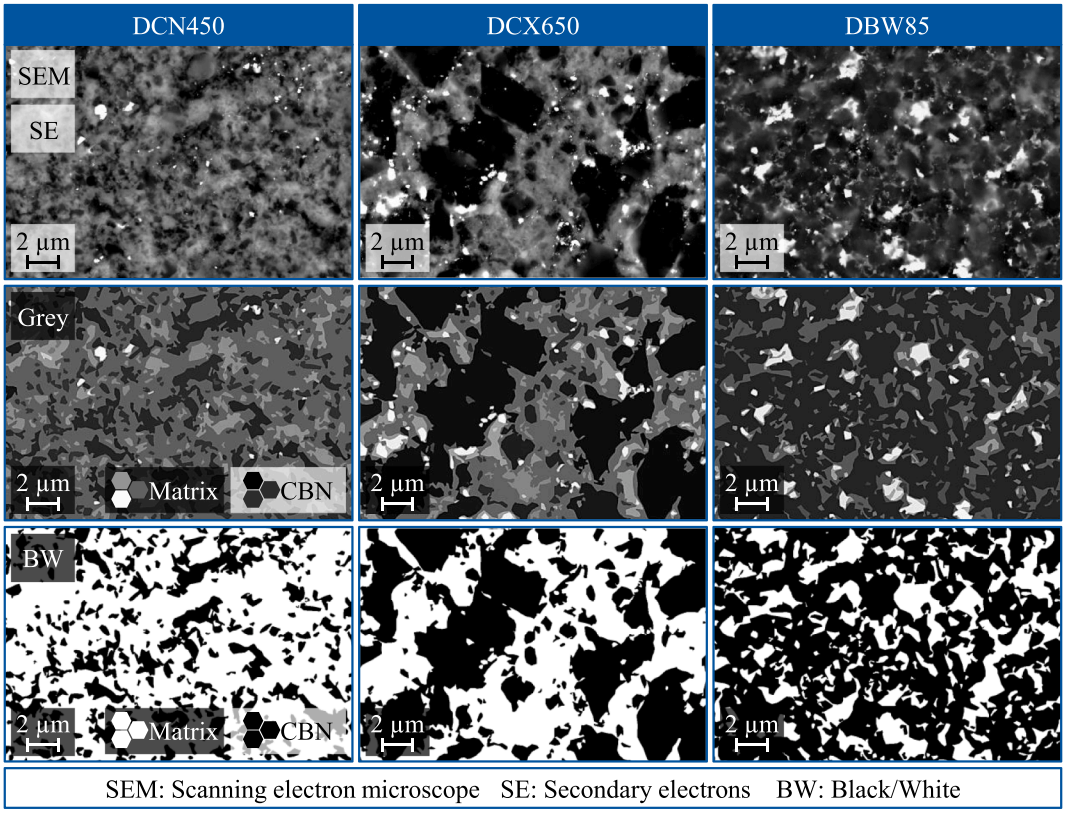

Appendix C. Table of coefficients for the friction model

pcBN specification	K(K_{Ic})	A(K_{Ic})	B(w_{cBN})
DCN450	0.008822853	4.563583456	0.0000516068
DCX650	0.045135958	0.997296814	0.000127717
DBW85	0.034134531	1.867516353	0.000212725

Appendix D. Deviation between the model output and the measured values

pcBN specification	Output variable	Relative velocity v_{rel} [m/s]		
		5	10	15
DCN450	Friction coefficient μ	6.7%	9.2%	8.6%
	Friction force F_f	8.1%	7.8%	9.3%
	Friction power P_f	8.1%	7.8%	9.3%
	Temperature T	2.9%	11.9%	17%
DCX650	Friction coefficient μ	16.6%	5.9%	6.9%
	Friction force F_f	16.1%	6.6%	8.9%
	Friction power P_f	16.1%	6.6%	8.9%
	Temperature T	8.5%	7.3%	14.2%
DBW85	Friction coefficient μ	3.2%	6.7%	8.2%
	Friction force F_f	4.7%	5.4%	8.7%
	Friction power P_f	4.7%	5.4%	8.7%
	Temperature T	5.6%	4.5%	4.6%

Appendix E. Crack propagation and cleavage on the MCD pin

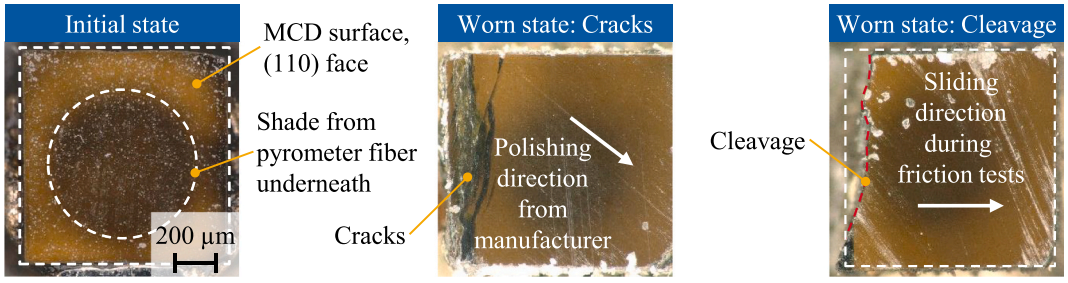

Appendix F. Microscope images of the pcBN-blanks before and after the friction tests

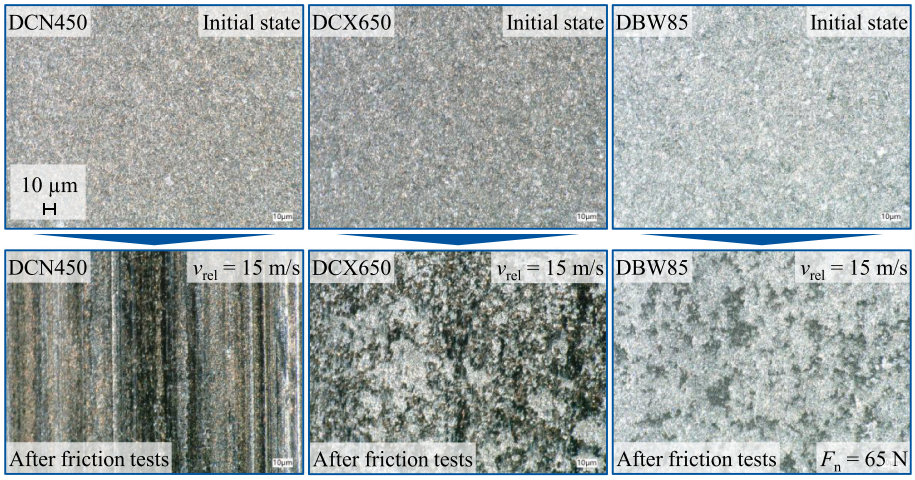

References

[1] Bobzin K. High-performance coatings for cutting tools. CIRP J Manuf Sci Tech 2017;18:1–9. https://doi.org/10.1016/j.cirpj.2016.11.004.
[2] Klocke F. Manufacturing processes 1. Springer; 2011. https://doi.org/10.1007/978-3-642-11979-8.
[3] Klimenko SA, Mukovoz YA, Polonsky LG. Cutting tools of superhard materials. Key Eng Mat 1995;114:1–66. https://doi.org/10.4028/www.scientific.net/KEM.114.1.
[4] Xi X, Ding W, Wu Z, Anggei L. Performance evaluation of creep feed grinding of c-TiAl intermetallics with electroplated diamond wheels. Chin J Aeronaut 2020;34:100–9. https://doi.org/10.1016/j.cja.2020.04.031.
[5] Li B, Dai C, Ding W, Yang C, Li C, Kulik O, et al. Prediction on grinding force during grinding powder metallurgy nickel-based superalloy FGH96 with electroplated CBN abrasive wheel. Chin J Aeronaut 2020. https://doi.org/10.1016/j.cja.2020.05.002. In-press [cited 2021 May 14].
[6] Ding X, Liew WYH, Liu XD. Evaluation of machining performance of MMC with pcBN and PCD tools. Wear 2005;259:1225–34. https://doi.org/10.1016/j.wear.2005.02.094.

[7] Sreejith PS, Krishnamurthy R, Malhotra SK. Effect of specific cutting pressure and temperature during machining of carbon/phenolic ablative composite using pcBN tools. J Mater Process Technol 2007;183:88–95. https://doi.org/10.1016/j.jmatprotec.2006.10.003.
[8] Bushlya V, Zhou J, Avdovic P, Stahl JE. Performance and wear mechanisms of whisker-reinforced alumina, coated and uncoated pcBN tools when high-speed turning aged Inconel 718. Int J Adv Manuf Technol 2012;66:2013–21. https://doi.org/10.1007/s00170-012-4477-5.
[9] Su H, Liu P, Fu Y, Xu J. Tool life and surface integrity in high-speed milling of titanium alloy TA15 with PCD/pcBN tools. Chin J Aeronaut 2012;25:784–90. https://doi.org/10.1016/S1000-9361(11)60445-7.
[10] Pierson H. Handbook of carbon, graphite, diamond and fullerenes. In: Properties, processing and applications. Noyes Press; 1993.
[11] Kress J. Auswahl und Einsatz von polykristallinem kubischen Bornitrid beim Drehen, Fräsen und Bohren [dissertation]. Dortmund: TU Dortmund University; 2007.
[12] Meyer R. Neue Schneidkantengeometrien zur Verbesserung des Werkzeugeinsatzverhaltens beim Hartdrehen [dissertation]. Hannover: Leibniz University Hannover; 2011.
[13] Ventura C. Manufacturing of cutting edge geometries on pcBN inserts by plunge-face grinding [dissertation]. Hannover: Leibniz University Hannover; 2014.
[14] Schindler F. Zerspanungsmechanismen beim Schleifen von polykristallinem Diamant [dissertation]. Aachen: RWTH Aachen University; 2015.
[15] Friemuth T. Herstellung spanender Werkzeuge. 1st ed. Düsseldorf: VDI; 2002.
[16] Mamalis AG, Horvath M, Grabchenko AI. Diamond grinding of superhard materials. J Mater Process Technol 2000;97:120–5. https://doi.org/10.1016/S0924-0136(99)00358-1.
[17] Behrens L. Grinding of pcBN [dissertation]. Hannover: Leibniz University Hannover; 2016.
[18] Mao C, Liang C, Zhang Y, Zhang M, Hu Y, Bi Z. Grinding characteristics of cBN-WC-10Co composites. Ceram Int 2017;43:16539–47. https://doi.org/10.1016/j.ceramint.2017.09.040.
[19] Haenel A, Hasterok M, Schwarz M, Schimpf C, Nestler A, Brosius A, et al. Investigation on the grinding characteristics of binderless nanocrystalline cubic boron nitride (BNNC) as cutting material for the machining of hardened steels and superalloys. Proc CIRP 2018;77:493–6. https://doi.org/10.1016/j.procir.2018.08.257.
[20] Denkena B, Grove T, Müller-Cramm D, Krödel A. Influence of the cutting direction angle on the tool wear behaviour in face plunge grinding of PcBN. Wear 2020:454–5. 203325, https://doi.org/10.1016/j.wear.2020.203325.
[21] Vits F, Trauth D, Mattfeld P, Vits R, Klocke F. Analysis of the tribological conditions in grinding of polycrystalline diamond based on single grain friction tests using the pin-disk principle. Key Eng Mat 2018;767:259–67. https://doi.org/10.4028/www.scientific.net/KEM.767.259.
[22] Bergs T, Mueller U, Vits F, Barth S. Tribological conditions in grinding of polycrystalline diamond. Diamond Relat Mater 2020;108:1–7. https://doi.org/10.1016/j.diamond.2020.107930.
[23] Vits F. Tribologie beim Schleifen von PKD [dissertation]. Aachen: RWTH Aachen University; 2020.
[24] Element Six Ltd. pcBN properties of DCN450, DCX650 and DBW85. (Requested on www.e6.com and approved for publication, May 2021).
[25] Proes F, Eichenseer C, Hintze W, Schell N, Leahy W, M'Saoubi R, et al. In situ analysis of PCBN cutting tool materials during thermo-mechanical loading using synchrotron radiation. Prod Eng Res Devel 2018;12:535–46. https://doi.org/10.1007/s11740-018-0791-6.
[26] ISO 13565-2. Geometrical product specifications (GPS) – surface texture: profile method; surfaces having stratified functional properties. 1996.
[27] ISO 8785. Geometrical product specifications (GPS) – surface imperfections – terms, definitions and parameters. 1998.
[28] Lawn BR, Padture NP, Cai H. Guiberteau F. making ceramics "ductile". Science 1994;263:1114–6. https://doi.org/10.1126/science.263.5150.1114.
[29] Bifano TG, Dow TA, Scattergood RO. Ductile-regime grinding: a new technology for machining brittle materials. J Eng Ind 1991;113:184–9. https://doi.org/10.1115/1.2899676.
[30] Heath P. Developments in applications of PCD tooling. J Mater Process Technol 2001;116:31–8. https://doi.org/10.1016/S0924-0136(01)00837-8.